Acta Crystallographica Section A
Foundations and Advances
ISSN 2053-2733

Received 19 August 2013
Accepted 13 December 2013

Symmetry of helicoidal biopolymers in the frameworks of algebraic geometry: α-helix and DNA structures

Mikhail Samoylovich[a]* and Alexander Talis[b]

[a]Central Scientific Research Institute of Technology 'Technomash', Ivan Franko Street 4, Moscow, 121108, Russian Federation, and [b]A. N. Nesmeyanov Institute of Organoelement Compounds of the Russian Academy of Sciences, Vavilova Street 28, Moscow, 119991, Russian Federation. Correspondence e-mail: samoylovich@technomash.ru

The chain of algebraic geometry and topology constructions is mapped on a structural level that allows one to single out a special class of discrete helicoidal structures. A structure that belongs to this class is locally periodic, topologically stable in three-dimensional Euclidean space and corresponds to the bifurcation domain. Singular points of its bounding minimal surface are related by transformations determined by symmetries of the second coordination sphere of the eight-dimensional crystallographic lattice E_8. These points represent cluster vertices, whose helicoid joining determines the topology and structural parameters of linear biopolymers. In particular, structural parameters of the α-helix are determined by the seven-vertex face-to-face joining of tetrahedra with the E_8 non-integer helical axis 40/11 having a rotation angle of 99°, and the development of its surface coincides with the cylindrical development of the α-helix. Also, packing models have been created which determine the topology of the *A*, *B* and *Z* forms of DNA.

1. Introduction

The secondary structure of a protein is largely determined by rigid covalent bonds in a polypeptide chain and by hydrogen bonds between its side groups. An important role is also played by steric interactions of molecules, related to their sizes and shapes, which impose strong structural limitations on the positions of molecules in space. Moreover, these interactions to a large extent determine the packing of molecules into helices, which are widespread in biological objects (Shulz & Schirmer, 1979; Finkelstein & Ptitsyn, 2002; Nelson & Cox, 2004). Ordered packings in three-dimensional Euclidean space E^3 are determined by constructions of algebraic topology (Conway & Sloane, 1999; Dubrovin *et al.*, 2001; Humphreys, 1975); hence it appears quite reasonable to put such constructions in correspondence with structures of helical biopolymers. Such a topological (packing) approach differs from the metric approach, which is founded based on exact geometric parameters of molecules and is widespread in biology (Chothia *et al.*, 1977). For example, in Samoylovich & Talis (2010) the use of such a construction allowed us to explain noncrystallographic structural features of certain crystals. Such constructions have also been used quite widely to reflect the symmetries of various molecular structures of biological objects (Monastyrsky, 2006).

Proteins can also be considered as a dense packing of more or less spherical units, amino acids, approximated by a packing of tetrahedra. The densest packing of regular tetrahedra is achieved in a four-dimensional polyhedron (polytope) {3, 3, 5} whose substructures (Figs. 1*a*, 1*b*) are related to the α-helix as shown by Sadoc & Rivier (1999) and Sadoc (2001). As is already known, the α-helix is a realization of the noncrystallographic axis 18/5 proposed by Pauling *et al.* (1951) with a rotation angle of 100° = 360°/(18/5). It has subsequently been shown that hydrogen bonds appear between the *i*th amide and (*i* + 4)th carbonyl groups of residues and stabilize the α-helix (Shulz & Schirmer, 1979; Finkelstein & Ptitsyn, 2002). However, even 60 years after the publication of Pauling's paper, a symmetry-based justification is still needed for the fact that there are precisely 3.6 amino-acid residues per turn in the α-helix. The same problem is also urgent for other biopolymers. In other words, the crystal is a joining of crystallographic space-group orbits, but which constructions of algebraic geometry and topology determine the symmetry of helical biopolymers?

In a general case, the (sub)structure of the biopolymer in question may be limited by a surface whose singular points are connected by symmetries of an algebraic polytope. Such a polytope is generated by a subsystem of the root lattice E_8. The E_8 lattice is the octonion lattice closing the series of possible numbers, *i.e.* real numbers – complex numbers – quaternions – octonions (Conway & Sloane, 1999).

A tetrahedron approximating the packing of four amino acids is a simplex in E^3, and the joining of tetrahedra (Fig. 1*b*)

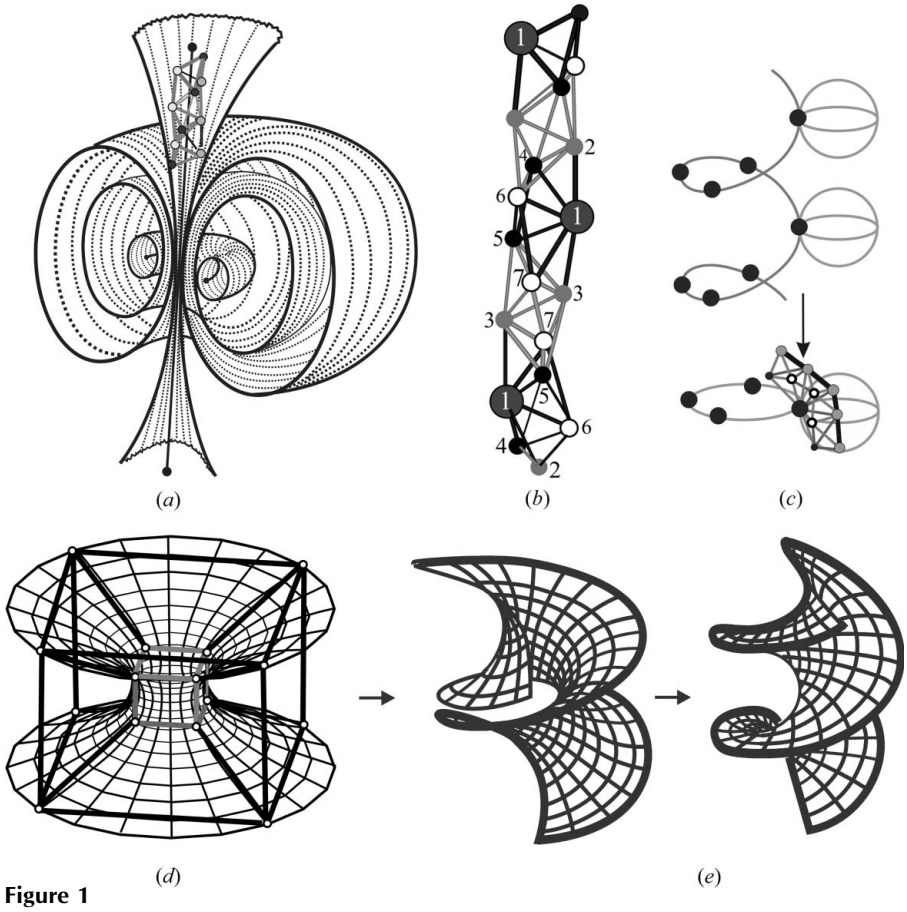

Figure 1
(*a*) A family of tori which are coaxial with the spherical torus. This family fills up the volume of the three-dimensional sphere S^3. The axis of the Boerdijk–Coxeter helix corresponds to the torus axis in the {3, 3, 5} polytope. (Adapted from Fig. 8 in Mosseri *et al.*, 1985.) (*b*) The Boerdijk–Coxeter helix obtained from regular tetrahedra. A simplicial seven-vertex complex of four tetrahedra with common vertex 1 is shown by black lines. Two such complexes are joined by a connected sum – the three tetrahedra between them (grey lines). (*c*) Representation of a cover over a bouquet of the circle S^1 and the sphere S^2 in the form of spheres attached to a screw line. On every sphere a solid common point with the screw line is shown, corresponding to a point of a manifold on S^1. This point is the common vertex joining two seven-vertex complexes (Fig. 1*b*). (Adapted from Fig. 103b in Dubrovin *et al.*, 2001.) (*d*) The projection of {4, 3, 3} polytope vertices on the catenoid (adapted from Fig. 9b in Mosseri *et al.*, 1985), which is determined by the family of tori (Fig. 1*a*). (*e*) The transformation of catenoid (Fig. 1*d*) into helicoid *via* an intermediate surface (wound over the catenoid) – joining of catenoid and helicoid surfaces. Trajectories of the generatrix ends are marked by thick lines. (Adapted from Fig. 26 in Fomenko & Tuzhilin, 1992.)

determines a simplicial complex (Dubrovin *et al.*, 2001). The connection between the simplicial (cellular) complex and its bounding minimal surface in E^3 is determined by a fibre bundle construction for the three-dimensional sphere S^3, in particular, in the form of a cover over a bouquet $S^1 \cup S^2$ of the circle S^1 and the sphere S^2 (Fig. 1*c*). Such a transition from the sphere S^3 (containing polytope vertices) is possible only by selecting on appropriate spheres certain manifolds and algebras characterizing these manifolds (Samoylovich & Talis, 2012*a*,*b*, 2013*a*,*b*). Polytopes are extrema of the volume functional, and locally minimal surfaces are also extrema of the volume functional. All lined minimal surfaces can be realized as a one-parameter family of helicoids with a pitch as a parameter (Fomenko & Tuzhilin, 1992). The line-geometric character of a minimal surface is the significant feature while using polyhedral constructions. A catenoid determined by one such surface is locally isomorphic to a helicoid (Figs. 1*d*, 1*e*).

In general, the above allows us to state the existence of a singular chain of algebraic geometry and topology constructions: an algebraic polytope insertable into the second coordination sphere of the E_8 lattice $\rightarrow$ the locally minimal surface $\rightarrow$ one-parameter family of helicoids $\rightarrow$ bundle (cover) with the fibre of cellular (simplicial) complexes $\rightarrow$ local-latticed packing of cell complexes. The existence of such a chain implies the possibility of realizing in E^3 a special class of helicoidal topologically stable structures. Belonging to this class means biological structures can avoid the crystalline type of order in E^3.

The apparatus of the generalized crystallography developed in the present work allows us to determine symmetries of helicoidal biopolymers by constructions of algebraic geometry and topology; these constructions define their assembly from quite a limited number of 'blocks' according to a very limited number of joining rules. The present article is devoted to the deduction of such a construction which determines *a priori* the structure parameters of the α-helix and symmetry parameters of certain forms of DNA.

2. Locally cylindric approximation of a rod substructure of a polytope

Each invariant of the root lattice E_8 is in correspondence with a certain disc D_0^2; hence construction of an algebraic polytope is actually determined by the relations

$$S^3 \cong D_0^2 \times S^1 \sim S^1 \cup S^2 \leftarrow \sum_j S_j^2, \qquad (1)$$

where $S^1 \cup S^2 \leftarrow \sum_j S_j^2$ is a cover over a bouquet $S^1 \cup S^2$ and the circle S^1 is correlative to a group $\{\exp i\varphi\}$ corresponding to a unitary representation. The sewing (glueing) operation defined in the cover (1) gives a law for joining the appropriate discs, and that law realizes an assembly of polyhedra into a rod. For simplicial (cellular) complexes, (1) can be rendered by a fibre bundle construction σ, for which the base σ_B and the fibre σ_F are represented by simplicial complexes:

$$\sigma \cong \sigma_B \times \sigma_F, \quad \partial\sigma \cong \sigma_B \times (\partial\sigma_F); \qquad (2)$$

the number of vertices of the simplicial complex in the fibre space equals the product of the number of vertices of the complexes of the fibre and the base (Fig. 1*c*).

For a minimal surface M, its stability is determined by the possibility of changing its area by small strains. The stability of M is characterized by the index Ind M, which correlates to the number of ways to change the surface area. If this index is not zero, the surface M is unstable. The instability of the M surface increases as the Ind M increases, which is equal to 1 for a catenoid and to ∞ for a helix (Figs. 1*d*, 1*e*). There are well developed methods to construct complete minimal surfaces, embedded in E^3, by using Weierstrass representations (Fomenko & Tuzhilin, 1992). Let M be some surface given by Weierstrass representation and $U \subset C$ is some subdomain of the complex plane. The surface M is characterized by Ind M = 0 if the image of the U is in some open submanifold of the S^2 sphere (Fomenko & Tuzhilin, 1992). That submanifold can be defined as a submanifold onto a part of the S^2 sphere (about 5/6 of the total sphere area) confined between two parallel planes. Indeed, such planes are separated from the sphere centre over the distance $\mathrm{th}t_0$, where t_0 is the unique root of the equation $\mathrm{cth}t_0 = t_0$, and cut off the domain of about 1/6 of the sphere surface area. For the $\{12(2^\gamma{\cdot}24)\}$ polytope given by $\{12(2^\gamma{\cdot}24)\}$ vectors of the second coordination sphere of the E_8 lattice ($\gamma = 0, 1, 2$), the submanifold of its 5/6 vertices defines the $\{10(2^\gamma{\cdot}24)\}$ or $\{12(2^\gamma{\cdot}20)\}$ polytope. This polytope can be mapped into polyhedra $\{2^\gamma{\cdot}24\}_q$ or $\{2^\gamma{\cdot}20\}_q$, ensuring the possibility of the existence of a surface with a finite (and possibly zero) value of Ind M.

It has been shown (Fomenko & Tuzhilin, 1992) that Weierstrass representations allow one to define a catenoid as well as a complete helicoid and, in the general case, an associated family for some minimal surface M consists of locally isometric minimal surfaces (incongruent pairwise, as a rule). At certain conditions one can create a configuration as a joining of helicoid and catenoid with the summary (total) radius-vector

$$r(u, \varphi, \alpha) = r_1(u, \varphi)\cos\alpha + r_2(u, \varphi)\sin\alpha, \qquad (3)$$

where r_1, r_2 are radius-vectors describing the catenoid and helicoid, (u, φ) are coordinates on the surface and φ corresponds to the angle in cylindrical coordinates. The angle $\alpha \in [0, \pi/2]$ is such that for $\alpha = 0$ the surface generatrix becomes a catenary (chain line) of the catenoid, and for $\alpha = \pi/2$ it becomes the generatrix of the helicoid (Fomenko & Tuzhilin, 1992).

A helicoid can be represented as infinite-sheeted winding over a catenoid or sphere without both poles. To describe all minimal surfaces tightening (spanning) the contour of two coaxial circles of radius r positioned in two parallel planes separated by a distance of h, it is sufficient to define all catenoids spanning this contour (Fig. 2*a*). For some fixed value of the angle α in (3) it is possible to build a construction that is a 'sum' of a catenoid with radius $r = \cos\alpha$ and a helicoid with distance between turns equal to $h = 2\pi\sin\alpha$. With decreasing interturn spacing at a certain value $h = h_{\rm cr}$ the bifurcation point arises. The value $h_{\rm cr}$ is given by the solution of the equation $\mathrm{cth}(h/r) = (h/r)$ (Fomenko & Tuzhilin, 1992). One can show that

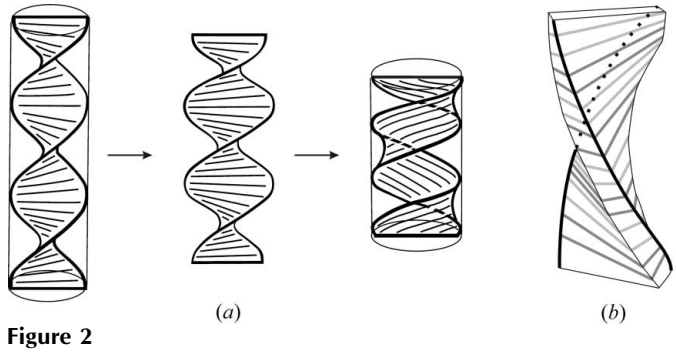

Figure 2
(*a*) A closed path consisting of two helices and two closing segments. The limiting cylinder of the system is shown by thin lines. Decreasing the pitch of the helix leads to a transformation of a helicoid into a double-helix helicoidal surface of the catenoid, uniting the mentioned subsystems (adapted from Fig. 27 in Fomenko & Tuzhilin, 1992). (*b*) Joining of rods by helicoidal law. The helical components of the double helix are shown by thick lines. (Adapted from Kléman, 1989.)

$$h_{\rm cr}/r = 2\pi\sin\alpha_{\rm cr}/\cos\alpha_{\rm cr} = 2\pi\tan\alpha_{\rm cr} \simeq 2\pi \times 0.382 \simeq 2.400, \qquad (4)$$

where $\alpha_{\rm cr} \simeq 20.906^\circ$, $\tan\alpha_{\rm cr} = h_{\rm cr}/2\pi r \simeq 0.382$. At $h = h_{\rm cr}$ the single whole configuration arises as a film which is tightening each of the parallel circles by the flat disc (Fig. 2*a*). After this the bifurcation point catenoid, determined by (3), decomposes into a stable cylinder and an unstable cone. In a bifurcation point (non-degenerate for a Morse function) a topological regularity is broken (Dubrovin *et al.*, 2001); at the same time a cell structure (considered in Fig. 1*c*) must appear on the manifold. Making a significant simplification, we shall assume that the relation (4) determines the transition from a locally minimal to a locally cylindrical surface, namely, the surface for which the neighbourhood of every point is approximated by a cylindrical surface.

The lattice E_8 determines both the {3, 3, 5} and {240} polytopes where the {240} polytope is the diamond-like joining of two {3, 3, 5} polytopes (Coxeter, 1930, 1973; Mosseri *et al.*, 1985) on the three-dimensional sphere S^3 (Figs. 1*a*, 1*d*). The polytope {240} starts the sequence $\{q(2^\gamma{\cdot}24)\}$, q is an integer, $\gamma = 0, 1, 2$, of polytopes (Samoylovich & Talis, 2012*a*,*b*, 2013*a*). The choice of the origin in a deep hole of the E_8 lattice determines the sequence of coordination spheres of 16, 128, 448 and 1024 vectors (Conway & Sloane, 1999). This allows one to select a subset of 1152 = 128 + 1024 vectors of the second coordination sphere E_8, corresponding to the polytope $\{1152\} = \{12(2^2{\cdot}24)\}$, whose substructures will be used in the following.

In the diamond-like $\{10(2^\gamma{\cdot}24)\}$ polytope $\gamma = 0, 1, 2$, the joining of $2\{q\}$ vertices on two neighbouring circles S^1 forms a Q chain, similar to a $\langle 110\rangle$ chain in a diamond structure. The maps of a Q chain into a Q edge of the 'loaded' polyhedron $\{2^\gamma{\cdot}24\}_q$ we shall denote by a two-headed arrow in Figs. 3(*a*–*c*). By these maps a three-dimensional rod substructure K of a diamond-like polytope corresponds to a face of the poly-

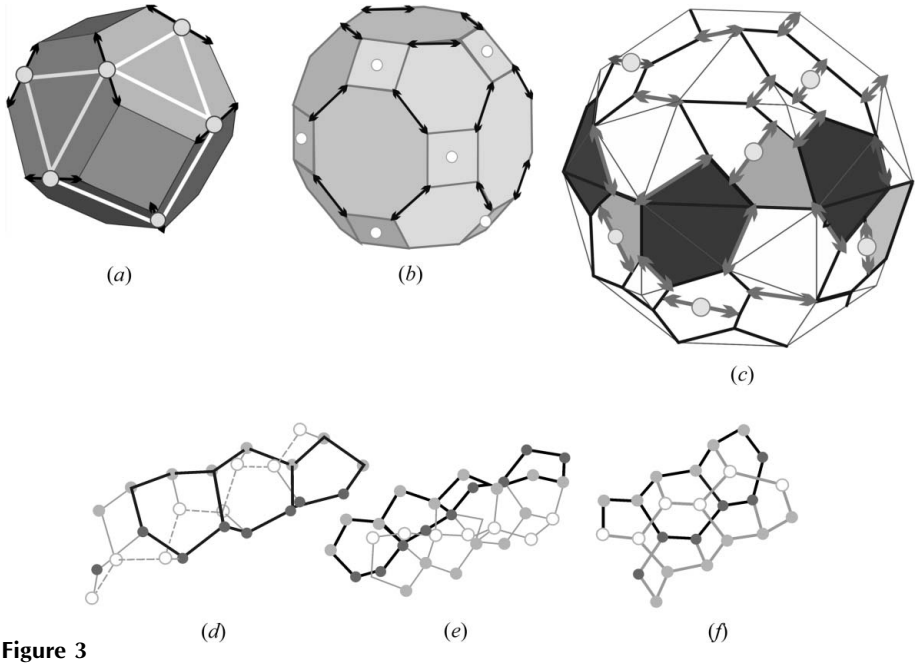

Figure 3
(*a*) A 24-vertex truncated octahedron with six square and eight hexagonal faces; the centres of 12 non-intersecting arrowed edges (cuboctahedron vertices) are shown as light dots. (*b*) A 48-vertex truncated cuboctahedron with 24 non-intersecting arrowed edges; the centres of 12 squares are shown as light dots. Square vertices are the arrow ends. (*c*) A 96-vertex simple polyhedron with 5-, 6- and 7-gons and 48 non-intersecting arrowed edges. Alternating 5- and 7-gons, denoted as light and dark shaded, form an equatorial belt; light dots denote the centres of 12 edges, each of which is common for two 5-gons. (*d*), (*e*), (*f*) Channels 30/11, 40/9 (adapted from Figs. 16a and 17 in Mosseri *et al.*, 1985) and 40/11, as joining of ⟨110⟩ diamond-like chains which correspond to hexagonal, square and octagonal faces, respectively, of the polyhedron in Fig. 3(*b*). Chains of hexacycles are shown by thick lines.

hedron $\{2^{\gamma}\cdot 24\}_q$. A diamond-like polytope {240} is determined by the relations $(30/11)^3 = -(40/9)^4 = (10/1)^1$ between motions in E^4, possessing rotational components (in one of two planes) by 132°, 81° and 36°, respectively. With mapping onto a sphere it corresponds to a joining of eight 30/11 channels, while six 40/9 channels appear in the interstices between the 30/11 channels (Fig. 3*a*). For a surface M, given by a Weierstrass representation (C, $f$dw, g), the index Ind M is finite provided that the function g is irrational (Fomenko & Tuzhilin, 1992). The symmetries 30/11 and 40/9 (Figs. 3*d*, 3*e*) are in correspondence with such functions (Samoylovich & Talis, 2007); hence, the minimal surfaces relevant to such non-integer axes will possess finite Ind M and in some degree topological stability. The {10(2·24)} polytope is next to the {240} polytope in the series, determined by the polyhedron $\{2\cdot 24\}_q$ (Fig. 3*b*), and is characterized by the relations

$$(30/11)^3 = (40/11)^4 = -(40/9)^4 = (10/1)^1, \qquad (5)$$

corresponding to appropriate rods (Figs. 3*d*, 3*e*, 3*f*). The negative sign denotes the different axis chirality.

The surface of the channel K in the neighbourhood of a point may be viewed as cylindrical; hence the homogeneity of a parametric description of a curve positioned on that surface permits a cylindrical approximation of the construction considered. In this case the centres of cell complexes (clusters) form a system of points on a helix, which may correspond to a two-dimensional lattice on the flat development of a cylinder, determined by one of the axes L/p of Gosset's helicoids:

$$L/p = 2^{\gamma}\cdot 8I_n/4k_{js}m_{js}, \qquad (6)$$

where $2^{\gamma}\cdot 8I_n$ and $8I_n$ are the number of vertices from the second or the first coordination spheres of the lattice E_8; $\gamma = 0, 1, 2$; I_n, $I_s = k_{js}(m_{js} + 1)$ are invariants of E_8, k_{js} are integers, m_{js} is the index of a lattice embedded in E_8 (Samoylovich & Talis, 2007, 2008, 2009). The value L/p, where p is a prime or some power of it, corresponds to an exponential representation $\exp 2\pi ip/L$ or one-parameter subgroup of the symmetry group of a polytope.

Thus, non-integer L/p axes (actually defined as one-parameter transformations) give the symmetries of discrete systems considered as homogeneous spaces represented by polytopes. Really, the transition (1) from the polytope onto S^3 to the discrete system as a cover over the union of spheres $S^1 \cup S^2$ forces a certain algebraic construction with p elements on S^1. Since the polytope is a four-dimensional object, these constructions must be relevant to the four-dimensional root lattices with the largest exponent being equal to 11 (for the F_4 system having roots corresponding to the roots of the first and second coordination spheres of the D_4 lattice). The last thesis should bring to addition the intermediate conditions in the form of $(\exp 2\pi/p)^p = 1$, thus permitting the realization of a periodicity.

According to Samoylovich & Talis (2012*a*,*b*, 2013*a*,*b*), the channel of the K type can be approximated by the orbit of a screw axis with a rotation angle of $2\pi p/L$ and a shift by the vector h along the axis in the case where the channel is formed by Q chains of the same type. This channel may determine a topologically stable (with some finite Ind M) helicoidal structure Ω which satisfies the relations

$$\Omega \leftarrow \langle L/p|\,\lambda h(r(u,\varphi,\alpha))\rangle 2\{q\} \leftarrow \{q(2^{\gamma}\cdot 24)\} \leftarrow E_8, \qquad (7)$$

where λ is an integer, $\gamma = 0, 1, 2$. According to (4), for $r(u, \varphi, \alpha) \simeq h/(2.400)$ the radius determined by (3) represents the radius of a cylindrical surface, into which Ω can be mapped. The angle of rotation of the L/p axis depends only on invariants of E_8; for instance, substituting in (6) $I_n = 20$, $k_{js} = 2$, $m_{js} = 11$, $\gamma = 1$ determines the axis 40/11. At the same time the local-lattice property is mapped depending on the direction of the rotation axis, as well as the magnitude h from the value $r(u, \varphi, \alpha)$.

An element of the crystallographic space group is determined by the relation (7) in the limiting case $L/p = n$, $n = 1, 2, 3, 4, 6$, and $h = t/n$, where t is a lattice vector D_3 (face-centred cubic lattice) or hexagonal lattice $A_2 \times A_1$. The lattice D_3 is

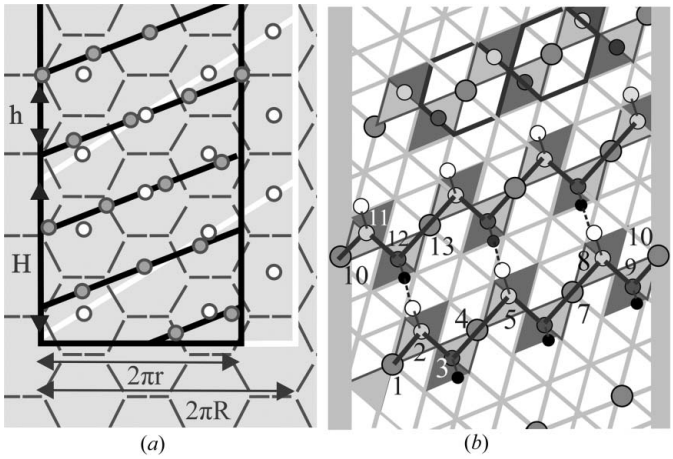

Figure 4
(*a*) A hexagonal network with the marked strip having a width of six unit edges of a hexagon; the white circles are the centres of regular hexagons. The white lines, where the centres of hexagons are positioned, constitute the flat development of a helix with a pitch $H \simeq 2(3^{1/2})$ (double hexagon height) and a radius R. The black lines within the strip of length $2\pi r \simeq 4.54$ represent the flat development of a helix with a pitch $h = H/2$. There are 40/11 black circles for every turn of the helix. (*b*) The dark-grey circles are centres of hexagons of the locally transformed hexagonal lattice, between which the dark-grey triangles are situated. They are the common vertices of pairs of light-grey triangles, the midpoints of whose edges contain light-grey and grey circles. The lines joining the light-grey and grey circles of adjacent chains contain white and black circles. The union of the circles nearest to each other determines the flat development of an α-helix, whose 13 consecutive vertices are marked by numbers.

embedded in the four-dimensional lattice D_4, from which the system G_2 can be obtained by quasi-decomposability (Humphreys, 1975), the said system G_2 is determined by the first and second coordination spheres of the hexagonal lattice A_2. For instance, for $L/p = 4$, $\lambda = 1$, $h(r(u, \varphi, \alpha)) = H = 2(3^{1/2})$ and $r = 3/\pi$ the cylindrical approximation Ω represents a helicoidal strip of regular hexagons sharing common edges (where the edge length is equal to 1), which includes half the hexagons of the flat development of a cylinder (Fig. 4*a*). The relation $h/r \simeq 2.400$ for such a helix is achieved only if it is turned into a helix 40/11 satisfying (7). In this case a helix with $L/p = 40/11$ is realized for $\lambda = 2$ and a radius decreasing to the value $r \simeq 0.722$, which gives the value $h = 3^{1/2} \simeq 2.400 \times 0.72$ (Fig. 4*a*).

3. Symmetry parameters of the α-helix in the frameworks of algebraic geometry

The conformation of the α-helix (Fig. 5*a*) is stable; hence all the above (with certain limitations) may be used for its cylindrical approximation, in which the centres of congruent elements of the packing coincide with the positions of C_α atoms. Generally accepted data concerning the structure of the α-helix (Finkelstein & Ptitsyn, 2002; Nelson & Cox, 2004) allow one to assume that L residues are equally distributed both over p turns of the 'main' helix, as well as over four helices, which we will call i-helices, $i = 1, 2, 3, 4$. Each of the i-helices corresponds to a linear substructure of hydrogen bonds; hence a cylindrical approximation of an α-helix (Figs. 5*b*, 5*c*) may be considered as a result of multiplication by a screw axis L/p of a starting i-helix of $L/4$ residues.

A non-integer axis, giving the experimental 3.6 residues per turn, is the axis $L/p = 18/5$. Because 18 is not divisible by 4, one must take a combined 36/10 helix consisting of two 18/5 helices (Fig. 5*b*) in order to obtain four i-helices with the same rotation angle. A non-composite axis of the form L/p, closest to 36/10, which can be obtained by adding four residues by turn, is the axis $40/11 = (36 + 4)/(10 + 1)$. That axis with helical rotations by 99° maps four i-helices onto each other (Fig. 5*c*). Here each i-helix contains ten residues. In contrast to 36/10, the axis 40/11 is expressed by a periodic decimal fraction and corresponds to the symmetry of the {10(2·24)} polytope (Figs. 3*b*, 3*f*), defined by the relation (5). The relation (5) implies that the orbit of the axis 40/11 is the union of the four orbits of the axis 10/1 (it is approximated by an axis close to the screw axis 10_1), which is also a relation between axes of the cylindrical approximation of the α-helix. The helix 40/11, ensuring the existence of the four i-helices, is followed by the helix 44/12 $= (40 + 4)/(11 + 1)$, which is the quadruple of the helix 11/3 (Fig. 5*b*). It is exactly 11/3 that corresponds to the average length of observed α-helices in globular proteins (Shulz & Schirmer, 1979). The one closest to 44/12 is the helix 45/12, which is a triple helix 15/4 with rotation by 96°.

The observed lengths of α-helices show relative maxima at 7, 11 and 15 residue lengths, thus corresponding to two, three and four turns (Shulz & Schirmer, 1979). They can be viewed as a result of separation of $40 = 7 + 7 + 11 + 15$ vertices of the helix $40/11 = 3.63(63)$, into cycles, situated on two, two, three and four turns. The substructures, put into correspondence with such cycles, may be characterized by axes 7/2, 7/2, 11/3 and 15/4. An arithmetic mean of these axes is the experimentally observed 18/5 axis, and its correspondence with the 40/11 axis:

$$(7/2 + 7/2 + 11/3 + 15/4)/4 = 3.60416(6) \rightarrow 18/5,$$
$$(7 + 7 + 11 + 15)/(2 + 2 + 3 + 4) = 3.63(63) \rightarrow 40/11. \quad (8)$$

Thus, relationships (8) connect the experimentally observed 18/5 axis of the α-helix (Pauling *et al.*, 1951) with the 40/11 axis of the ideal (mathematical) α-helix (rotation angles are 100 and 99°, respectively).

A distribution of residues in an α-helix into 11 turns and local inserting of the {10(2·24)} polytope into the E_8 lattice allows the suggestion of an availability of the symmetrical construction which can define these conditions. As it happens, such a construction is the 2-(11, 5, 2) scheme of block design or biplane (Kostant, 1995; Brown, 2004): 11 numbers from 0 up to 10 are subdivided on blocks by five numbers in each (below, the number 10 is denoted by the roman numeral X). The blocks are selected in such a way that each number belongs to five blocks, each pair of numbers to two blocks, and every collection of four numbers to one block only. An automorphism group (of order 660) of the biplane is the group $PSL_2(11)$, a limiting group of four special groups $PSL_2(p)$, $p = 3, 5, 7, 11$ determined by Galois (Conway & Sloane, 1999; Kostant, 1995; Brown, 2004).

Let us distribute 11 blocks of biplane so that the 55 numbers contained in them form a matrix B of 11 rows and five columns, presented in Fig. 5(d). In the first column 1, 2, 3 . . . 9, X, 0 form the sequence of positive integers which are indexing 11 rows. After skipping the first column there remains the W matrix of size 11 × 4. The third, sixth, ninth and 0th rows of the W matrix contain the number 1, its skipping leaves these rows with three numbers in each and distributes 40 elements of the $W(a, b)$ matrix into 11 rows. These 40 elements $W(a, b)$, $a = 1, 2, \ldots, X, 0$; $b = 1, 2, 3, 4$ are distributed between four W_i subsets of the matrix (ten for each):

$$W_i = \sum_{n,m} W((n + 3m - \delta_{m3}), (i + m) \pmod 4), \quad (9)$$

where $(n + 3m - \delta_{m3})$ is the row number, and $(i + m)$ (mod 4) is the column number in the W matrix, $i = 1$, 2, 3, 4; $n = 1, 2, 3$; $m = 0, 1, 2, 3$; $\delta_{m3} = 1$ for $m = 3$ and 0 for $m \neq 3$ (Fig. 5d). The rows of the W matrix are in one-to-one correspondence with the turns of the cylindrical plane development of the helix 40/11, and i-sets (9) to i-helices, $i = 1, 2, 3, 4$ (Figs. 5c, 5d); therefore, at a combinatorial level (without metrics) the substructure W of a biplane B may be identified with a flat development of a cylindrical approximation of an α-helix.

In fact, in the biplane any four or three numbers belong to just the given block; therefore, the presence of three or four numbers in any row of the matrix 11 × 4 (and, therefore, the number of C_α atoms in a turn) is stable in the combinatorial sense. The skipped unit numbers subdivide 11 rows of the matrix W into superblocks: 11 = 3 + 3 + 3 + 2; at the same time, in a superblock of three rows there will be 11 numbers (11 residues by three turns), which correspond to the already mentioned median length 17 Å for observed lengths of α-helices in globular proteins. Without the three top block ones, there are 30 numbers in the eight remaining rows of the W matrix, thus corresponding to the 30/8 = 15/4 axis. Within a superblock there are no intersections of rows by two numbers, which ensures its combinatorial stability. At the same time, rows from two different superblocks intersect by two numbers, which allows one to consider the possibility of glueing an α-helix through atoms corresponding to these common pairs of numbers.

The helix 10/1 is common to the channels 40/11 and 30/11 [determined by (5)], which is possible if they are both defined according to the same law. In fact, by analogy with the definition of the cylindrical flat development 40/11 from the biplane B, the flat development for 30/11 may be obtained from B by skipping the first two columns and three unities 1 in the remaining columns. At that, the remaining 30 = 55 − 2 × 11 − 3 numbers may also be distributed into three ten-element subsets of the form (9).

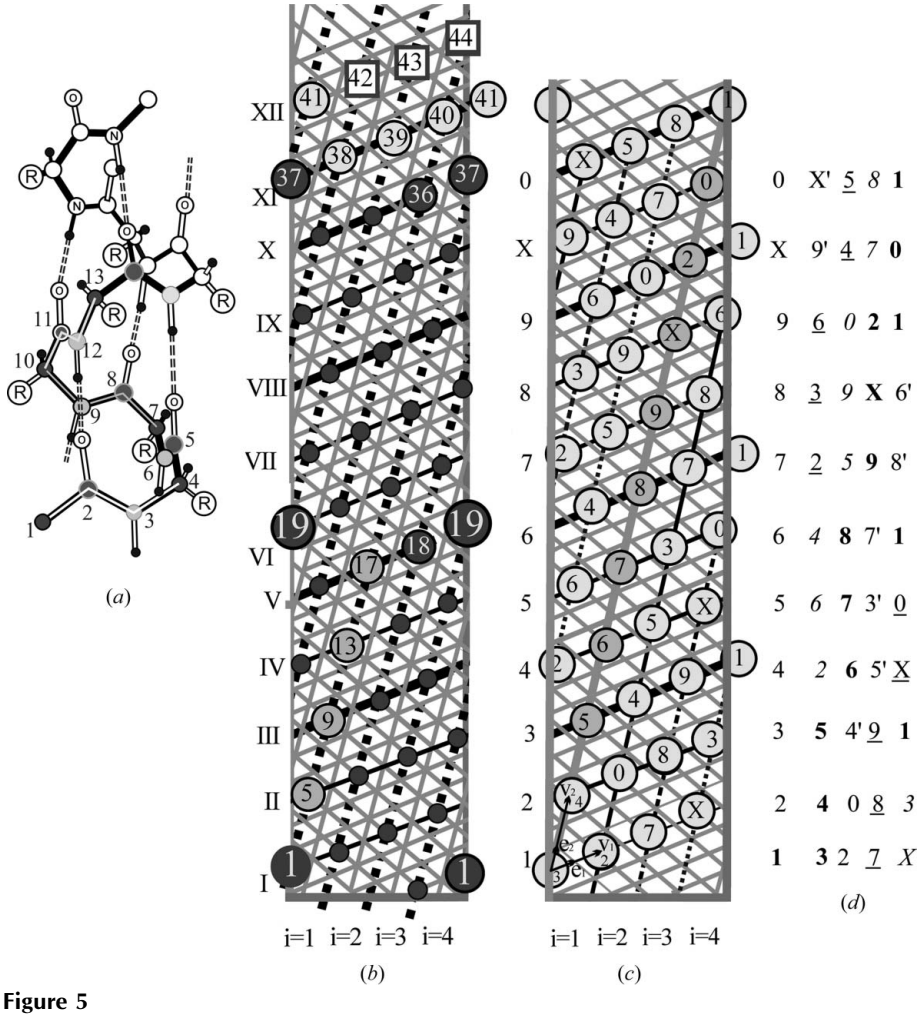

Figure 5
(*a*) The structure of an α-helix, pendant groups are designated by the letter R, hydrogen bonds are shown by a dotted line (adapted from Fig. 7-5 in Finkelstein & Ptitsyn, 2002). Dark-grey, grey, light-grey, white and black balls represent, respectively, C_α, C′, N, O and H atoms in the packing. (*b*) The development of a locally cylindrical approximation of the α-helix having the 36/10 axis shown in Fig. 5(*a*). Forty-four C_α atoms are disposed on 12 turns designated by roman numerals. Atoms with equal numbers are identified. Each turn designated by the thick line contains three atoms, each of the remaining turns contains four atoms. Atoms i and $i + 4$ belong to one of the four dotted straight i lines, $i = 1, 2, 3, 4$ (taking into account for identifying the vertical edges of the stripe). (*c*) The development of a locally cylindrical approximation of the α-helix having a 40/11 axis. The development is inserted into the lattice with basic vectors e_1 and e_2 and the sublattice with basic vectors V_1 and V_2. (*d*) Biplane 2-(11, 5, 2) as the matrix 11 × 5 with 11 lines by five numbers in each line. The first column of biplane numbers is the number of turns on the development in Fig. 5(*c*). Skipping 1 out of the matrix corresponds to the distribution of C_α atoms over turns and i straight lines in Fig. 5(*c*), i lines are marked as thick, thin, dashed and dotted ones. The numbers corresponding to straight lines $i = 1, 2, 3, 4$ are shown as bold, primed, underlined and italic, respectively.

4. The α-helix is the structure determined by the helical joining of tetrahedra

In addition to the helical 18/5 rotation (close to 40/11), basic parameters characterizing the structure of an α-helix are (in Å): pitch $h = 5.4$ and radius $r = 2.3$ (Shulz & Schirmer, 1979). The relation $h/r \simeq 2.349$ satisfies the condition (4), confirming the necessity of application of the formalism being developed here in order to derive structural parameters of the α-helix.

Let us put the origin of coordinates (0, 0) into a point v_0 of the plane development of a cylindrical approximation of the α-helix (Fig. 5*c*). According to (7), the point v_0 is connected to the point v_1 *via* the vector V_1 with coordinates $2\pi r/(40/11)$, $h/(40/11)$, and v_0 is connected to v_5 by the vector V_2 with coordinates $2\pi r/10$, $4(h/(40/11))$. The angle χ between those vectors is determined by the relation

$$\cos\chi = (1 + (10C/(11 + C^2))^2)^{-1/2}, \qquad (10)$$

where $C = 2\pi/c_{cr} = c\tan\alpha_{cr}$, $c_{cr} = h/r \simeq 2.400$ in accordance with (4). For $c \simeq 2.46 \simeq 6^{1/2}$ one obtains for the vector length the relationship $V_2 = (3/2)V_1$, thus permitting us to define the vectors with the same length $e_1 = (1/2)V_1$ and $e_2 = (1/3)V_2$ and the angle $\chi \simeq 55^\circ$ between them. Considering the vectors e_1 and e_2 as the basis, it is possible to construct a lattice $\{e_1, e_2\}$, which will contain a sublattice $\{V_1, V_2\}$ with basis vectors V_1 and V_2. For $h = 5.4$ Å the strip $\{V_1, V_2\}_\alpha$ of the lattice $\{V_1, V_2\}$ almost coincides with the flat development of a cylindrical approximation of the α-helix for C_α atoms (Fig. 5*c*). Vectors (in particular, the Darboux vector) giving the curvature and the torsion of the curve (Dubrovin *et al.*, 2001), approximating the C_α helix, are in correspondence with elements of the algebra g_2, but are not in the basis of its lattice. Using the formalism mentioned in Dubrovin *et al.* (2001), it can be shown that the strip $\{e_1, e_2\}_\alpha$ corresponds to a system of vectors determined by a Chevalley group of type G_2, representing a generalization of a group of type G_2 over local and commutative rings (Humphreys, 1975; Bunina, 2012). Thus, the channel 40/11 of a polytope allows us to define a strip of hexagons, embedded into the lattice A_2, and then to construct a strip of the lattice $\{e_1, e_2\}_\alpha$ which contains the sublattice $\{V_1, V_2\}_\alpha$, corresponding to a flat development of a cylindrical approximation of the α-helix for C_α atoms.

In the transition (1) of the sphere S^3 to the universal covering $\sum_j S_j^2$ over bouquet $S^1 \cup S^2$, the circle S^1 serves as the base and the sphere S_j^2 the jth fibre (Fig. 1*c*). Sphere S_j^2 is the universal covering of the projective plane; therefore, the simplicial complex σ_j which corresponds to the jth layer may be determined by the finite projective geometry PG $(2, n)$. The incidence graph of PG $(2, n)$ is a regular map on the torus $\{6, 3\}_{q,1}$, and dual to it – the map on the torus $\{3, 6\}_{q,1}$ containing seven vertices, 21 edges and 14 triangular faces (Coxeter, 1950). Skipping from $\{3, 6\}_{q,1}$ six edges and four triangles leads to the irregular map $\{3, 6\}^6_{q,1}$ on the sphere that can be inserted into the lattice A_2 (Samoylovich & Talis, 2013*a*,*b*). Ten regular triangles of $\{3, 6\}^6_{2,1}$ provide all the vectors of the G_2 system (Fig. 6*a*); therefore, a PG $(2, n)$ is sufficient to take a minimal finite projective geometry PG (2, 2). The irregular $\{3, 6\}^6_{q,1}$ map corresponds to the development of the seven-vertex joining of four regular tetrahedra in a face-to-face mode, representing a simplicial complex.

Thus, a helix of simplicial complexes may be obtained upon transition (in a cover over a bouquet) from the base S^1 to a

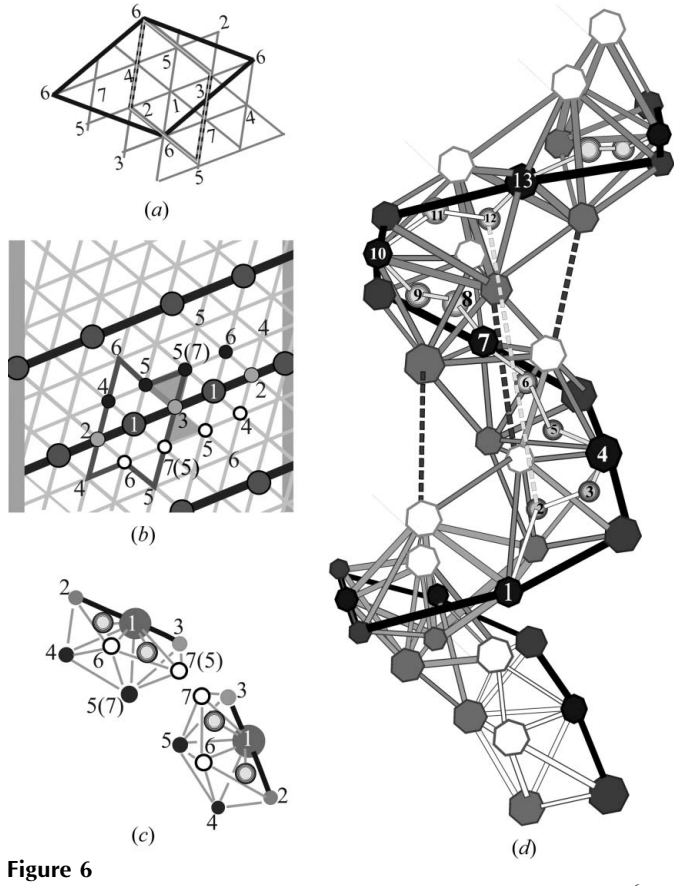

Figure 6
(*a*) The map $\{3, 6\}_{2,1}$ contains ten triangles of the irregular map $\{3, 6\}^6_{2,1}$ in the rhombus, which is shown by double lines. The triangles 3–5–7 and 2–4–6 are shown by dotted lines. (*b*) The development of a locally cylindrical approximation of the α-helix having the 40/11 axis (Figs. 4*b*, 5*c*) as the joining of maps $\{3', 6\}^6_{2,1}$. The numbers of vertices of isosceles triangles $\{3'\}$ coincide with the numbers of regular triangles $\{3\}$ in Fig. 6(*a*). The triangles 3–5–7 are common to two neighbouring maps; they are the dark-grey triangles in Fig. 4(*b*). (*c*) Identifying the vertices with equal numbers of map $\{3, 6\}^6_{2,1}$ in Fig. 6(*a*) determines a seven-vertex face-to-face joining of four regular tetrahedra with the common vertex 1. Two such joinings of four regular tetrahedra may be united (as manifolds) by their common face 3–5–7. Shaded spheres are placed in the interior of 1–2–4–6 and 1–3–5–7 tetrahedra. (*d*) The helix packing of the seven-vertex joining of tetrahedra (collected by their faces of the type 3–5–7), which is determined by identifying equal vertices of the flat development in Fig. 6(*b*). White edges delineate the seven-vertex joining of four tetrahedra which is shown in the bottom part of Fig. 6(*c*). The black edges join the black centres of the seven-vertex joining of four tetrahedra and dark-grey vertices. They form a helix, determined by the 40/11 axis. The white and light-grey vertices (white and black in Figs. 1*c*, 6*b*, 6*c*) form two other 40/11 helices. The vertices included in the 4_{13} cycle of the α-helix (vertices of type 1 and shaded spheres in Fig. 6*c*) are numbered in accordance with (13) and Figs. 5(*a*), 4(*b*). The white dotted line, which closes the 4_{13} cycle, connects vertices 2 and 12. Atoms O and H disposed on this white dotted line and realizing the hydrogen bond are not shown. The white dotted line is parallel to the dotted line connecting the nearest white and light-grey vertices.

discrete system of points on the helix 40/11, and from the fibre S_j^2 to the simplicial complex σ_j:

$$S^1 \rightarrow \langle 40/11\rangle v_0 \leftrightarrow \{V_1, V_2\}_\alpha,$$
$$S_j^2 \rightarrow \sigma_j \rightarrow \mathrm{PG}(2,2) \rightarrow \{3', 6\}^6_{2,1} \leftarrow \{e_1, e_2\}, \qquad (11)$$

where $\langle 40/11\rangle = \langle 40/11|11h/40\rangle$ is a helical rotation by an angle of $99^\circ = 11 \times 360^\circ/40$ with a shift along the axis by $11h/40$. Upon mapping (11), the base point j, where the complex σ_j is 'attached', maps into the node V_j of the strip $\{V_1, V_2\}_\alpha$, which is also the centre of a flat development of the map $(\{3', 6\}^6_{2,1})_j$ of ten isosceles triangles (Figs. 6*a*, 6*b*). Correspondingly, a cylindrical approximation of the α-helix with pitch $h = 5.4$ Å and radius $r = 2.3$ Å is determined by the relationships

$$\langle 40/11\rangle^j(\{3', 6\}^6_{2,1})_1 \cong (\{3', 6\}^6_{2,1})_{1+j},$$
$$(\{3', 6\}^6_{2,1})_j \cap (\{3', 6\}^6_{2,1})_{j+1} = \{3'\}, \qquad (12)$$

where the centre of the map $(\{3', 6\}^6{}_{2,1})_j$ coincides with the jth C_α atom and the triangle $\{3'\}$ is common to two neighbouring maps $\{3', 6\}^6_{2,1}$. It is formed by the vectors e_1 and e_2 with an angle $\chi \simeq 55^\circ$ between them (Fig. 6*b*).

The simplicial complex $(\{3', 6\}^6_{2,1})_j$ is a joining of four tetrahedra sharing a vertex V_j, which represent the simplicial complex σ_j from the relationship (11). This is a special complex since it is inserted (by insignificant deformations) into an icosahedron, as well as into the Coxeter–Bordijk helicoid of regular tetrahedra (Figs. 1*b*, 6*c*). A face-to-face joining of two seven-vertex simplicial complexes $\{3', 6\}^6_{2,1} \cup \langle 40/11\rangle\{3',6\}^6_{2,1}$ is the 11-vertex complex (Fig. 6*c*), which corresponds to three α-helix turns, forming a superblock of its development (Figs. 5*c*, 5*d*). It may be put into correspondence with the helicoid 11/3 (Fig. 5*b*). One of its vertices is the common point for S^1 and S^2 in a cover over a bouquet (Fig. 1*c*). Discarding four points common for S^1 and S^2 while uniting according to the law (1), four such 11-vertex complexes allow one to obtain 40 points, corresponding to the orbit 40/11. Thus, the relations (11) and (12) determine a packing of simplicial complexes, satisfying the requirement of topological stability as well as experimental data concerning the structure of the α-helix (Shulz & Schirmer, 1979; Finkelstein & Ptitsyn, 2002). In other words, the structure parameters of an α-helix are determined by a packing of (almost regular) tetrahedra that appears upon multiplying (12) a special seven-vertex tetrahedra joining by a non-integer axis of helical rotation 40/11 (Fig. 6*d*).

The C_α atom (positioned in a common vertex of the four tetrahedra joining) is four-coordinated, and it determines positions of the N and C′ atoms inside the 'external' tetrahedra of the whole joining at the left and right sides from C_α (Figs. 7–5 in Finkelstein & Ptitsyn, 2002). Such decoration of the simplicial complex (Fig. 6*c*) gives rise to formation of the ith link $(N–C_\alpha–C')_i$ of a polypeptide chain and ensures the assembly of these chains into the α-helix:

$$-(N - [C_\alpha - C')_i - (N - C_\alpha - C')_{i+1} - (N - C_\alpha - C')_{i+2} - (N - C_\alpha - C')_{i+3} - (N - C_\alpha] - C')_{i+4} -, \qquad (13)$$

in which C_α from the ith complex is linked to C_α from the $(i + 4)$th complex by the transformation $\langle 10/1\rangle = \langle 40/11\rangle^4$. Since 10/1 connects the starting and ending C_α, the starting N_1 and ending C_5' atoms belonging to the set of five links (N, C_α, C′) must be skipped. The 13-atom cycle of C_α atoms is denoted by square brackets. The carbon atoms $(C_\alpha)_1$ and $(C_\alpha)_5$ linked to C_1' and N_5 are tetra-coordinated, a physical bond between them is impossible, and hence instead of $(C_\alpha)_1$ and $(C_\alpha)_5$ the atoms O_1 and H_5 (also connected with C_1' and N_5) enter in this cycle. A bond between the atoms O_1 and H_5 is possible, and it closes the cycle 4_{13} of 13 atoms, which traditionally characterizes the α-helix (Fig. 5*a*).

The mapping of a polypeptide chain (13) by a flat development of a packing of tetrahedra presents a chain of isosceles triangles with common vertices C_α (Fig. 4*b*). At the same time, the atoms C′ and N are positioned on the midpoints of the bases of these triangles (or in other positions selected by symmetry in triangles). On each of the lines joining C'_i and N_{i+4}, $i = 1, 2\ldots$, there are two positions, selected by the symmetry of the $\{e_1, e_2\}$ lattice and which correspond to positions of the atoms O_i and H_{i+4}. According to (12) and (13), the shortest distance between the C_α atoms is determined by the transformation $\langle 40/11\rangle^1$, and the second distance between the C_α atoms by the transformation $\langle 40/11\rangle^4 = 10/1$. Thus, the characterizing α-helix 13-vertex 4_{13} cycle is determined by the parametric $\langle 40/11\rangle$ axis:

$$4_{13} = \left\{ \bigcup_{i=0}^{4} \langle 40/11\rangle^i (N, C_\alpha, C')_1 | N_1 = C_5' = 0, \right.$$
$$\left. (C_\alpha)_1 \rightarrow O_1 \cup H_5 \leftarrow (C_\alpha)_5 = \langle 10/1\rangle (C_\alpha)_1 \right\}. \qquad (14)$$

The number 13 in the designation of the cycle as 4_{13} actually gives the number of atoms in a cycle, while 4 must be determined as the degree of the axis $\langle 40/11\rangle$, mapping the ith C_α atom into the $(i + 4)$th C_α atom. Thus, the relationships (12) determine a helix packing of tetrahedra (Figs. 6*a*–6*d*), satisfying the requirement of topological stability as well as experimental data concerning the structure of the α-helix (Shulz & Schirmer, 1979; Finkelstein & Ptitsyn, 2002).

Within our approach the α-helix corresponds to a substructure of the {10(2·24)} polytope which is mapped into an octagonal face of the truncated cuboctahedron. Thus, the joining of its three closest octagons (Fig. 7*a*) is in correspondence with a superhelix formed by the α-helices, whose symmetry is determined by the symmetry of a polytope. A scheme of the superhelix is shown in Fig. 7(*b*) (adapted from Fig. 11-3 in Finkelstein & Ptitsyn, 2002). Within the triple of α-helices, which is characterized by the axes 40/11 and corresponds to the octagons in Fig. 7(*a*), there appears a channel, which is characterized (parametrically) by the axis 30/11 and corresponds to the hexagon in Fig. 7(*a*). At the same time, between pairs of channels 40/11 there are channels 40/9 appearing, which are in correspondence with squares (Fig. 7*a*). Similar relations may also be obtained for other superhelices as joining of α-helices.

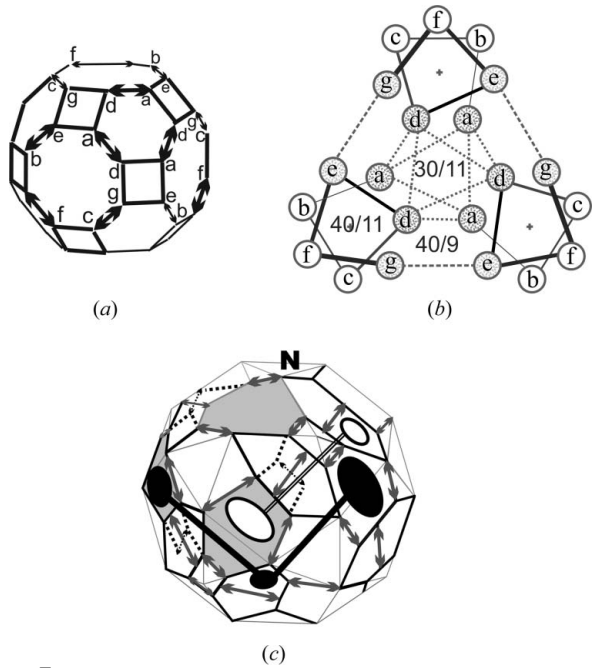

Figure 7
(*a*) A truncated cuboctahedron (Fig. 3*b*) with letters marking out seven vertices of the nearest to each other octagonal faces. (*b*) The scheme of the superhelix composed from three α-helices (adapted from Fig. 11-3 in Finkelstein & Ptitsyn, 2002) shown as *a*–*b*–...–*g* helices and corresponding to octagonal faces in Fig. 7(*a*). The channels appearing in the interior of three helices and between α-helix pairs correspond to hexagonal and square faces in Fig. 7(*a*). (*c*) The polyhedron (Fig. 3*c*) with $2^2{\cdot}24$ vertices and 12 heptagons, 24 pentagons, and 8 + 6 hexagons (of two types) as faces. Three grey heptagons around a hexagon appear by transforming three octagons in Fig. 7(*a*). This transformation is effected by 90° rotations of dotted arrowed edges. Black and white ovals single out parts of zigzag chains composed from three pairs of pentagons and heptagons. The 'north' pole of the polyhedron is designated by the letter N.

5. Constructions defining the symmetry parameters of DNA structures

Mapping of the symmetry of DNA structures requires interpretation of the double helix as a single object. For instance, the ends of rods, which join by the helical law, form a double helix, but a rod is a single object. Two half-turns of each end of rod arise after rotation of the rod by 180° (Fig. 2*b*). In order to describe a joining of two half-turns (as manifolds) from each helix of DNA structures with the formation of the united helical system (the *M* manifold), it is necessary to use a standard topological operation of taking a connected sum (Fig. 1*b*). In particular, such an operation as glueing of a handle (Dubrovin *et al.*, 2001) is applied in the α-helix for the assembly of seven-vertex tetrahedra joining. Application of the said operation plays a special role for the rod structures in question, because it provides an experimentally established possibility of bending them under certain angles (Nelson & Cox, 2004; Morozov *et al.*, 2009). In the structure of DNA the repeating elements in molecular packings are apparent in coding features (Nelson & Cox, 2004). In general, such structures are determined by a helical, scaled, ordered packing of large molecules; hence, to describe them one must use a local-lattice packing, which is capable of ensuring the repetition of molecule (cluster) centres both on each turn, and on each [similar to (14)] cycle.

A lattice (in the algebraic sense) is not necessarily defined as a subgroup of *n*-dimensional real space, generated by *n* linearly independent (ordinary) vectors. It is possible to use complex and quaternion vectors, because, besides whole real numbers, there are also three rings of whole numbers: Gaussian ones $\{(a + ib),\ a, b \in Z\}$, Eisenstein ones $(\{a + i\omega),\ a, b \in Z,\ \omega = (-1 + i/3^{1/2})/2\}$ and Hurwitz quaternion ones. In fact, the E_8 lattice may be described as the real part $\Lambda_{\rm real} = E_8$ of the Hurwitz lattice in H^2; at the same time for Hurwitz's one in H the lattice is $\Lambda_{\rm real} = D_4$. For the Gaussian two-dimensional one $\Lambda_{\rm real} = Z^2$ is a square lattice and for Eisenstein's one $\Lambda_{\rm real} = A_2$ is a hexagonal lattice. Such relations simplify a transition from using vector manifolds and automorphisms of the E_8 lattice to corresponding elements of polytopes and then to partitioning of the two-dimensional sphere or torus. Using 24-element groups, represented, as a rule, by two (differing only by sign) sets of 12 elements, allows one to use Mathieu groups M_{24} and M_{12}, which is realized in this work.

Let us consider the possibility of building some DNA structures based on a combinatorially (symmetrically) and topologically stable construction, in which an α-helix is realized. In view of the above discussion, such a construction must correspond to the angle of the helical rotation 40/11, a sequence of polytopes $\{10(2^{\gamma}{\cdot}24)\}$, $\gamma = 0, 1, 2$, from the second coordination sphere E_8; the group $PSL_2(11)$, the Chevalley group of type G_2 and the relationship $h/r \simeq 2.400$ of the pitch of the helix to its radius. In addition to structural features of the α-helix, this construction must take into account the double-helix nature of DNA structures and be typical of its local-lattice packing.

The axis 40/11 maps the triples of C_α, C′ and N atoms into each other, while the atoms belonging to the same triple do not map into each other. Let us assume that all C′ and N atom centres are projected onto the helix containing the C_α atom centres, and any two adjacent atom centres are mapped into each other by the same transformation (with the accuracy up to a conjugation). The mappings (projected onto a helix) of the C_α and C′, C′ and N, N and C_α atoms are in correspondence with three non-unit involutions in the Chevalley group of G_2 type.

As a result of tripling the number of homogeneous elements, this helix will be mapped onto itself by the non-integer 120/11 = (40 × 3)/11 axis with a rotation angle of 33°. The non-integer 120/11 helix axis coincides practically with the 11 = 121/11 axis, having 11 transitive elements per one turn. For an α-helix the ratio $h/r \simeq 2.400$ corresponds to the bifurcation point of the catenoid, so it is permitted to define (after several steps) a helix and, respectively, a double helix given by the ends of the helix generatrix (Fig. 2*b*). The possibility of doubling the number of α-helix elements has been presented in a previous consideration.

In particular, the subgroup $PSL_2(11)$ of the Mathieu group M_{11} acts on two orbits [1,11; 1,11] which may be put into

correspondence to a homogeneous distribution by 11 elements and one fixed point for each turn of the double helix (Conway & Sloane, 1999). The construction satisfying all the said conditions is the *A* form of DNA (Ivanov & Minchenkova, 1994), for which the ratio of the helix pitch to its radius (28.6 Å/11.5 Å $\simeq$ 2.487) is comparable with the topological stability criterion value of $h/r \simeq 2.400$ for a single helix. The significant difference of the *A* form from other forms of DNA is a shift of base pairs by 4–5 Å from the helix axis towards its periphery, which is supposedly related to various configurations of a sugar ring of deoxyribose. Actually, in a certain sense the *A* form is topologically (locally) closer to an incomplete Scherk surface, given by an appropriate Weierstrass representation for the local structure of the minimal surface. The given surface is also characterized by an instability index, but its formation is also related to additional requirements. In particular, the conditions of an exterior metric introduction are broken and there appears a necessity to use functions representable as a sum of functions of each variable (Fomenko & Tuzhilin, 1992). Thus, due to the absence of the central part of this surface, the *A* form does not belong to the most topologically stable forms of DNA structures.

By conserving all preceding concepts the use of the S_5 subgroup of the M_{11} group determining the action over the manifold [1, 5, 6; 2, 10] the said manifold can be associated with five and six elements on two half-turns of a single helix (with one fixed point) and two fivers (with two fixed points) on two half-turns of the second helix. In this case, there appears the possibility of joining [1, 5, 6; 2, 10] $\cup$ [2, 10; 1, 5, 6] of the half-turns of both helices, which forms the double helix, containing ten and 11 elements, respectively, in two adjacent turns of each helix. At that there are 21 elements per two turns, thus constituted by 10.5 elements per one turn, as is characteristic of the *B* form of DNA (Nelson & Cox, 2004).

The *A* form of DNA, defined previously, has been obtained by formal tripling of the α-helix *via* transition from the 40/11 to the 120/11 axis. At that, the second triple helix complementing the first one up to a double helix has been introduced by combinatorial reasoning. At the end of §4 the possibility has also been considered of the α-helix tripling by joining of three α-helices into the superhelix. This superhelix corresponds to three octagons around a hexagon of the polyhedron {2·24} (Figs. 7*a*, 7*b*). In the polyhedron $\{2^2{\cdot}24\}$ such joining corresponds to the union of three (grey) heptagons around the hexagon (Fig. 7*c*). The polyhedron $\{2^2{\cdot}24\}$ arises as a result of the degeneracy discarding (doubling) of the {2·24} polyhedron vertices. Because of this it can contain a substructure corresponding to the doubled helix. A hexagon, situated at the north (south) pole of the polyhedron $\{2^2{\cdot}24\}$, is in the centre of a zigzag-like equatorial union of three heptagons (and three pentagons between them), not sharing common vertices with them. Two such zigzag unions around the axis, joining the north and south hexagons, appear at the equator of the polyhedron $\{2^2{\cdot}24\}$ out of the white and black zigzag-like chains (Fig. 7*c*). Upon selecting on a sphere 'the north and south' discs (around the north and south hexagons) and subsequently glueing the discs, while allowing for a local cylindrical approximation of the minimal surfaces in question, two equatorial zigzag-like chains may be put into correspondence with half-turns of two helices, forming the double helix (Figs. 7*b*, 8*b*). Upon mapping a polytope onto a polyhedron, two points of a polytope correspond to a single point of the polyhedron (Mosseri *et al.*, 1985); hence lifting degeneration in E^3 must correspond to the appearance of two additional half-turns of two helices.

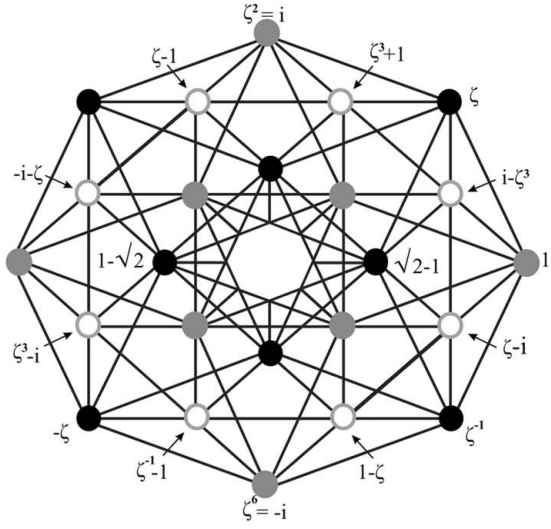

(*a*)

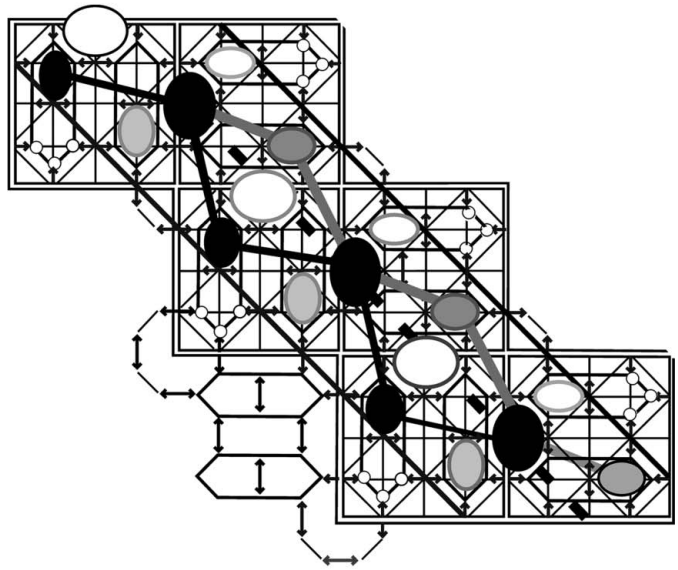

(*b*)

Figure 8
(*a*) The mapping of the {3, 4, 3} polytope onto a plane with the polytope vertices as elements of a nonprincipal lattice (adapted from Fig. 8.1 in Conway & Sloane, 1999). The colour shows the subdivision of 24 vertices onto three orbits of an eight-cyclic group and onto six orbits of a four-cyclic subgroup of the eight-cyclic group. (*b*) The flat development of the $\{2^2{\cdot}24\}$ polyhedron as a 96-vertex subdivision of the flat development of a cube into 5-, 6 - and 7-gons. Black (white) ovals single out a zigzag chain composed from three pairs of pentagons and heptagons. The congruent chains are denoted by black–grey and white–(light-grey) ovals. These chains are within the central strip shown by black lines, which corresponds to the 'equatorial' strip of the polyhedron in Fig. 7(*c*). The glide reflection plane is shown by a dotted line.

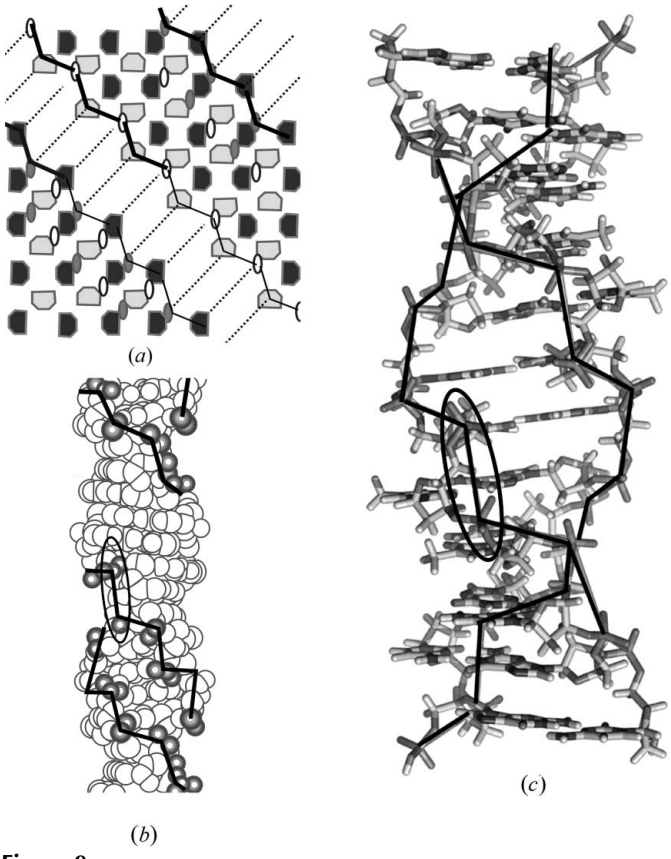

Figure 9
(*a*) The cylinder development of a double helix as part of the crystallographic tiling of zigzag chains, which is defined by the central strip of flat development in Fig. 8(*b*). Half-turns of helices are shown by thin and solid lines. Zigzag lines determine two left (relative to Figs. 5*a*, 5*b*) helices containing six pairs of pentagons and heptagons. In each pair a heptagon (pentagon) corresponds to a nucleotide in a *syn*-conformation (*anti*-conformation) in *Z*-form DNA (Saenger, 1983). (*b*) The repeated unit of the left-helix *Z*-form DNA is two adjacent nucleotide pairs; one pair is marked by an oval. The helix rotation angle is equal to -9° or -51°, which is dependent on the realization of the contact type (*anti–syn*-conformations or *syn–anti*-conformations) in the given point (adapted from Saenger, 1983). (*c*) A model of the *Z* form of DNA; the zigzagged double helix is shown by thick black lines. Two neighbouring nucleotide pairs are marked by an oval. (Adapted from a figure by Richard Wheeler, nickname Zephyris.)

A lattice over the ring of cyclotomic integers of the form $Z[\zeta]$, where $\zeta = \exp \pi i/4$, $\zeta^2 = i$ and $\zeta^4 = -1$, is a variant of the real lattice D_4; hence 24 vertices of the projection of the {3, 4, 3} polyhedron onto a plane may be represented by elements from $Z[\zeta]$ (Fig. 8*a*). The latter may be identified with the 24 vectors D_4 for the first and second coordination spheres. The two given classes of 24 vectors are included in the factor-manifold $D_4/3D_4$, which (beside the zero class) also contains 32 classes with three vectors in each (Conway & Sloane, 1999). In general, in the classes mentioned there are $\{2^\gamma \cdot 24\}$ vectors, which may be put into correspondence with vertices of polyhedra $\{2^\gamma \cdot 24\}$, $\gamma = 0, 1, 2$. According to Samoylovich & Talis (2009) the flat development of the $\{2^2 \cdot 24\}$ polyhedron may be obtained from 96-vertex partitioning of the flat development of a cube into 5-, 6- and 7-gons. It can be shown that this development may be obtained by projection onto a plane honeycomb {3, 4, 3, 3}, which contains polytope {3, 4, 3} as a cell (Fig. 8). There is a glide reflection plane $\{m|2a\}_{1/2}$ going through the midpoints of edges of the Petri polygon of the cube, making the six heptagons contained in them coincide. If one draws a glide reflection plane $\{m|2a\}_{1/4}$ going through quarters of edges of the Petri polygon and parallel to the given plane, it will bring to coincidence the centres of three pentagons and three heptagons. Joining of such polygons closest to each other, forms zigzag lines out of alternating pentagons and heptagons: black–black (black–grey), white–white [white–(light-grey)] chains (Fig. 8*b*). Thus, we get a flat development of equatorial zigzagged chains of the polyhedron $\{2^2 \cdot 24\}$, which correspond to a topologically stable local cylindrical approximation of the minimal surfaces and subsets of the local lattice $Z[\zeta]$.

The equatorial zigzagged chains considered above determine the flat development of a double helix, where for each turn there is a zigzag joining of six pairs of elements not congruent to each other (Fig. 9*a*). The said six pairs form a set of 12 elements with simultaneously six imprimitive two-element sets (heptagon–pentagon pairs) and two six-element sets (six heptagons and six pentagons), which are denoted by the symbol 6×2. The two turns of the double helix are in correspondence with two orbits $[6 \times 2, 6 \times 2]$ where the subgroup $2 \times S_5$ of the group M_{12} is acting. In a zigzagged chain of one helix each heptagon is connected to a pentagon and *vice versa*. A similar type of connection is preserved also while linking pentagons and heptagons closest to each other from different helices. Summing up the above, it is possible to assert that putting into correspondence with pentagons and heptagons of the flat development of the double helix the *syn*- and *anti*-conformations of the bases (Saenger, 1983), one obtains a scheme flat development of the *Z* form of DNA (Figs. 9*b*, 9*c*).

6. Conclusion

While the exact geometry of biological helices may appear complicated, their topology is determined simply and directly by steric considerations. The different types of structures in proteins, primary, secondary or tertiary, are related to close-packed structures in one, two or three dimensions (Sadoc & Rivier, 1999). The densest packing of regular tetrahedra is achieved in a four-dimensional polytope {3, 3, 5}, which is determined by an eight-dimensional lattice E_8. The diamond-like union of the two polytopes {3, 3, 5} – polytope {240} (Coxeter, 1930) starts the sequence $\{10(2^\gamma \cdot 24)\}$, $\gamma = 0, 1, 2$, of polytopes determined by the second coordination sphere of E_8. We have shown that structural parameters of the α-helix are determined by helix packing of seven-vertex unions of tetrahedra, which correspond to helical axis 40/11 from polytope $\{10(2 \cdot 24)\}$. This tetrahedral packing determines triangular packing on the surface, which corresponds to the bifurcation point for a minimal surface given by Weierstrass representation and satisfies the condition that the index of an unstable surface equals zero. The approximation of this surface by a cylindrically similar surface determines one-to-

one correspondence between the considered tetrahedral packing and close-packing of triangular maps $\{3', 6\}^{6}_{2,1}$ embedded in a triangular lattice rolled on a cylinder. Thus, we defined two-dimensional and three-dimensional ideal (mathematical) helices, which have exactly the topology of the α-helix. Within our approach, joining of α-helices forms a superhelix whose symmetry is determined by the symmetry of the polytope $\{10(2{\cdot}24)\}$.

This approach, which we are developing, shows that the necessary condition of stability and reproducibility of the biological structures studied is their correspondence to the unique system of constructions of algebraic geometry and topology. The mathematical description of the world is based upon a delicate interplay of the continuous and the discrete (Arnold, 1984); therefore the given condition determines the possibility of assembling atoms (molecules) according to topological properties of the real physical world and the conditions for existence (being embedded in it) of finite discrete ordered structures. As predicted by a theory of catastrophes (Arnold, 1984), the formation of such structures corresponds to processes of lifting configurational degeneration, and state stability – with the existence of a bifurcation point. We have mainly discussed the α-helix, but there are other biopolymers related to this approach, for instance, the topology of the *A*, *B* and *Z* forms of DNA determined by special helix local-lattice packings and symmetries of the $\{10(2^{2}{\cdot}24)\}$ polytope. Furthermore, in the case of DNA structures nature apparently makes a 'double check' with respect to the possible effects of crystallization – the local-lattice property is used for lattices defined over rings of algebraic whole numbers and not just over the customary ring of integers.

DNA structures not only contain the necessary functional code (a four-letter code with three-letter words, which corresponds to a requirement for a non-integer number of elements per turn), but also realize a very important transition from local-lattice atomically generated structures to local-lattice packings of molecules. Scale invariance of the system (a most general type of fractal transformation) is set into action by a certain local transformation (transition), where the repetition (local atomically generated lattice property) in chains and the number of elements transforms into the characteristic of the axis of a helicoidal rod, and then also into elements of a helicoidal local-lattice packing.

Ignoring local periodicity leads to formal breakdowns of the basic paradigm of biological reductionism (Sverdlov, 2006), because there have been cases, experimentally observed, when different proteins or the same protein with varying functions were coded by the same gene with a certain sequence of bases. This irregularity could have been ignored, were it not for a characteristic partition of the original DNA helix into separate subsystems, for instance, when reading the information. An important characteristic of DNA is the virtual double half-turn nature (which defines a 'building block' of the double helix as a union of two half-turns of each helix) of the turn of the helix. Worth noting also is the virtual half-turn nature of each turn, as well as a possible role of a hidden triple period in relation to using a three-letter basis (for a four-letter alphabet), when it is exactly three nucleotides that determine the type of amino acid in the formation of polypeptide chains. The fourth nucleotide cannot be unique due to its structural features, but it is necessary to take into account the role of RNA structures in changes of DNA.

At the present time, structural classification of proteins is based on bioinformatics, which uses possibilities afforded by computer enumeration and allows one to directly compare proteins not listing the constructions of algebraic geometry and topology that determine symmetry (Finkelstein & Ptitsyn, 2002). The formalism used in this work (whose detailed mathematical foundation is presented in Samoylovich & Talis, 2012*a*,*b*, 2013*a*,*b*) allows one, before resorting to real or computer experiments, to discover symmetry regularities of the structure of certain classes of biopolymers, which determine the possibility of *a priori* selection of topologically stable structures and symmetry classification of biopolymers.

It would be of interest to understand what new perspectives in the biophysics of DNA structures can occur (for example, on the part of evolution and functional changes of the genome) when the established topological features of their structure are taken into account, in particular, the stability of such systems and their subsystems, as well as substitution mechanisms for packing elements. Note also such features as an interconnection of local cylindrical nature with the frequently used cylindrical approximation; a special role of the local-lattice property and bifurcations in stability considerations; and the necessity to take into account parametric properties of non-integer axes and the virtual double-half-turn nature of a turn of the helix. In fact, the latter two characteristics undoubtedly change upon transitions from a state of a unified two-helix system toward separate one-helix fragments, for instance, upon methylation of nucleotide pairs. Finally, it should be established which molecular constructions correspond to special variants of the resulting surface, representing a union of the helicoid and the catenoid in the form of the helicoid wound over the catenoid.

References

Arnold, V. I. (1984). *Catastrophe Theory*. New York: Springer-Verlag.
Brown, E. (2004). *Math. Mag.* **77**, 87–100.
Bunina, E. (2012). *J. Algebra*, **355**, 154–170.
Chothia, C., Levitt, M. & Richardson, D. (1977). *Proc. Natl Acad. Sci. USA*, **74**, 4130–4134.
Conway, J. H. & Sloane, N. J. A. (1999). *Sphere Packings, Lattices and Groups*, 3rd ed. New York: Springer-Verlag.
Coxeter, H. S. M. (1930). *Philos. Trans. R. Soc. London Ser. A*, **229**, 329–425.
Coxeter, H. S. M. (1950). *Bull. Am. Math. Soc.* **56**, 413–456.
Coxeter, H. S. M. (1973). *Regular Polytopes*. New York: Dover Publications.
Dubrovin, B. A., Novikov, S. P. & Fomenko, A. T. (2001). *Modern-Day Geometry*. Moscow: Editorial URSS.
Finkelstein, A. V. & Ptitsyn, O. B. (2002). *Protein Physics*. Amsterdam: Academic Press.
Fomenko, A. T. & Tuzhilin, A. A. (1992). *Translations of Mathematical Monographs*, Vol. 93, *Elements of the Geometry*

and Topology of Minimal Surfaces in Three-Dimensional Space. Providence: American Mathematical Society.
Humphreys, J. (1975). *Linear Algebraic Groups.* New York: Springer-Verlag.
Ivanov, V. I. & Minchenkova, L. E. (1994). *Mol. Biol.* **28**, 780–788.
Kléman, M. (1989). *Adv. Phys.* **38**, 605–667.
Kostant, B. (1995). *Not. Am. Math. Soc.* **42**, 959–968.
Monastyrsky, M. I. (2006). Editor. *Topology in Molecular Biology.* New York: Springer-Verlag.
Morozov, A. V., Fortney, K., Gaykalova, D. A., Studitsky, V. M., Widom, J. & Siggia, E. D. (2009). *Nucleic Acids Res.* **37**, 4707–4722.
Mosseri, R., DiVincenzo, D., Sadoc, J. & Brodsky, M. (1985). *Phys. Rev. B*, **32**, 3974–4000.
Nelson, D. L. & Cox, M. M. (2004). *Lehninger Principles of Biochemistry*, 4th ed. New York: W. H. Freeman and Co.
Pauling, L., Corey, R. B. & Branson, H. R. (1951). *Proc. Natl Acad. Sci. USA*, **37**, 205–211.
Sadoc, F. J. (2001). *Eur. Phys. J. E*, **5**, 575–582.
Sadoc, F. J. & Rivier, N. (1999). *Eur. Phys. J. B*, **12**, 309–318.
Saenger, W. (1983). *Principles of Nucleic Acid Structure.* New York: Springer-Verlag.
Samoylovich, M. I. & Talis, A. L. (2007). *A Foundation for the Theory of Symmetry of Ordered Nanostructures.* Moscow: CNITI 'Technomash'.
Samoylovich, M. I. & Talis, A. L. (2008). *Dokl. Phys.* **53**, 292–297.
Samoylovich, M. I. & Talis, A. L. (2009). *Crystallogr. Rep.* **54**, 1117–1127.
Samoylovich, M. I. & Talis, A. L. (2010). *Acta Cryst.* A**66**, 616–625.
Samoylovich, M. I. & Talis, A. L. (2012*a*). *ArXiv*: 1211.3686.
Samoylovich, M. I. & Talis, A. L. (2012*b*). *ArXiv*: 1211.6560.
Samoylovich, M. I. & Talis, A. L. (2013*a*). *ArXiv*: 1303.4228.
Samoylovich, M. I. & Talis, A. L. (2013*b*). *Crystallogr. Rep.* **58**, 523–530.
Shulz, G. E. & Schirmer, R. H. (1979). *Principles of Protein Structure.* New York: Springer-Verlag.
Sverdlov, E. D. (2006). *Her. Russ. Acad. Sci.* **76**, 339–351.